ChemPubSoc Europe

DOI: 10.1002/open.201900169

Open Access ChemistryOPEN Full Papers

# Convection-Flow-Assisted Preparation of a Strong Electron Dopant, Benzyl Viologen, for Surface-Charge Transfer Doping of Molybdenum Disulfide

Keigo Matsuyama,[a] Akito Fukui,[a] Kohei Miura,[a] Hisashi Ichimiya,[a] Yuki Aoki,[a] Yuki Yamada,[a] Atsushi Ashida,[a] Takeshi Yoshimura,[a] Norifumi Fujimura,[a] and Daisuke Kiriya*[a, b]

Transition metal dichalcogenides (TMDCs) have received attention as atomically thin post-silicon semiconducting materials. Tuning the carrier concentrations of the TMDCs is important, but their thin structure requires a non-destructive modulation method. Recently, a surface-charge transfer doping method was developed based on contacting molecules on TMDCs, and the method succeeded in achieving a large modulation of the electronic structures. The successful dopant is a neutral benzyl viologen ($BV^0$); however, the problem remains of how to effectively prepare the $BV^0$ molecules. A reduction process with $NaBH_4$ in water has been proposed as a preparation method, but the $NaBH_4$ simultaneously reacts vigorously with the water. Here, a simple method is developed, in which the reaction vial is placed on a hotplate and a fragment of air-stable metal is used instead of $NaBH_4$ to prepare the $BV^0$ dopant molecules. The prepared $BV^0$ molecules show a strong doping ability in terms of achieving a degenerate situation of a TMDC, $MoS_2$. A key finding in this preparation method is that a convection flow in the vial effectively transports the produced $BV^0$ to a collection solvent. This method is simple and safe and facilitates the tuning of the optoelectronic properties of nanomaterials by the easily-handled dopant molecules.

Transition metal dichalcogenides (TMDCs) are attractive for use in developing atomically thin optoelectronic devices due to TMDCs' flat crystalline surface at a sub-nanometer thickness;[1–3] their possessing band gaps;[4,5] and their chemical,[4,5] mechanical,[6] and electrical durability.[7] Various optoelectronic applications, such as metal-oxide-semiconductor field-effect transistors (MOSFETs),[1,8] tunnel FETs,[9] optical sensors,[10] photovoltaics,[11] and light-emitting diodes,[12] have been demonstrated. Further advancement of these high-performance semiconducting devices requires modulating the carrier concentrations of the TMDC body.[1,5] However, the thin structural nature of the TMDCs makes it difficult to control carrier concentrations via established methods, such as ion implantation, as they may destroy the crystalline lattice.

Surface charge-transfer doping methods were recently developed to modulate the carrier concentration of TMDCs.[3,5] The method uses molecules,[13–17] polymers,[18] inorganic compounds[19] or alkali metals[20] that contact the TMDC surface and transfer electrons from either material to the other. Of the dopants studied, one of the strongest and air-stable dopant is the benzyl viologen (BV) molecule.[15] The BV molecule is known as a redox-active molecule, which exhibits two electron-transfer systems between divalent ($BV^{2+}$), monovalent ($BV^+$), and neutral isomer ($BV^0$) (Figure 1a).[21] The important point is that the

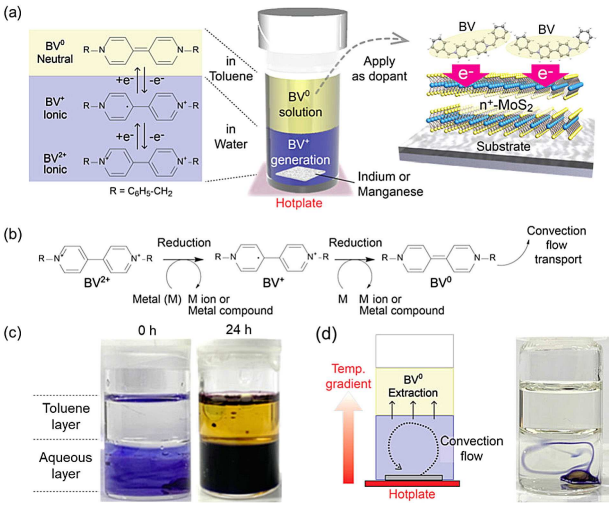


**Figure 1.** (a) Illustrative image of the synthesis/purification system of the strong electron dopant, BV molecule. The $BV^0$ molecule is generated and transported to the upper toluene layer, which shows a strong electron doping ability for $MoS_2$. (b) Plausible reduction scheme of BV with metal plates. (c) The macroscopic pictures of the solution at 0 h and 24 h of the reaction on a hotplate at 60 °C with an indium plate. The solutions are bubbled with $N_2$ gas. (d) Visualization of the convection flow generated from the indium plate at 60 °C. The reaction solution is not bubbled with $N_2$ gas beforehand.

[a] K. Matsuyama, A. Fukui, K. Miura, H. Ichimiya, Y. Aoki, Y. Yamada, Prof. A. Ashida, Prof. T. Yoshimura, Prof. N. Fujimura, Prof. D. Kiriya
Department of Physics and Electronics, Osaka Prefecture University, 1–1 Gakuen-cho, Naka-ku, Sakai-shi, Osaka 599-8531, Japan
[b] Prof. D. Kiriya
PRESTO, Japan Science and Technology Agency (JST), 4-1-8 Honcho, Kawaguchi, Saitama 332-0012, Saitama, Japan
E-mail: kiriya@pe.osakafu-u.ac.jp

Supporting information for this article is available on the WWW under https://doi.org/10.1002/open.201900169

neutral isomer of the $BV^0$ molecule shows a strong electron-donor ability.[21–23] Previously, $BV^0$ molecules were found to be able to dope electrons to a typical TMDC, $MoS_2$, and convert the $MoS_2$ from a semi-conductive to a metallic state.[15] Contrary to the usefulness of the reducing ability, a redundant process to use the $BV^0$ molecule is synthetic procedure. In a reported process, $BV^0$ molecules are synthesized from a chloride form of BV ($BV^{2+}$ isomer; benzyl viologen dichloride) by reduction with sodium borohydride ($NaBH_4$) in an aqueous solution.[21] The generated BV molecule is a neutral isomer ($BV^0$) and extracted in a binary toluene layer on the aqueous solution. The $NaBH_4$ reacts vigorously with the water and from this vigorous reaction generates a large amount of hydrogen gas while simultaneously reducing $BV^{2+}$ to $BV^0$ isomer. The powder form of $NaBH_4$ is also redundant in terms of the handling process due to its hygroscopic nature, and it requires sufficient safety guideline due to its relatively high reducing ability.

An easy-handling, safe, and effective method for producing and using $BV^0$ molecules without $NaBH_4$ should be attractive for developing TMDCs for use in optoelectronic devices. Here, we demonstrate a simple strategy for synthesizing $BV^0$ molecules from a $BV^{2+}$ aqueous solution by reduction with indium or manganese metal fragments (Figure 1a, and 1b). The system consists of bilayer solutions of bottom aqueous $BV^{2+}$ solution and upper toluene; after dropping the metal into the solution, the reaction is gradually progressed on a hotplate at 60 °C. The $BV^0$ can be extracted and separated from the source $BV^{2+}$ by extracting the upper toluene layer (Figure 1a, and 1c). The toluene solution shows the strong doping ability of $MoS_2$ MOSFET as previously reported. In addition to the simplicity of the method used for generating $BV^0$, extraction mechanism is also important for the effective preparation of the $BV^0$ molecules. On the hotplate at 60 °C, a non-equilibrium convection flow was governed by the temperature distribution between the bottom and the top of the vial (Figure 1d). The synthesized neutral $BV^0$ molecules (hydrophobic in character) were transported effectively from the bottom aqueous solution to the upper toluene by the convection flow. In the extraction and transportation process, other isomers of $BV^{2+}$ and $BV^+$ in water were separated. This work facilitates using a strong electron dopant to modulate nanoelectronic materials such as graphene,[23] TMDCs[15] and carbon nanotubes[21] via a simple process with the aid of a synthesis-purification protocol with a non-equilibrium convection flow.

We first examined the reduction process of $BV^{2+}$ in an aqueous solution with an indium fragment. An indium plate (~ 5 mm × 5 mm) was dropped into the binary solution of toluene and $BV^{2+}$ aqueous solution (Figure 2a). $N_2$ bubbling was applied to the reaction solution in advance, because the generated radical form of $BV^+$ isomer would react with oxygen molecules (see below).[24] The reaction was progressed on a hotplate at 60 °C, and an orange toluene solution of $BV^0$ molecules was obtained as in the previous $NaBH_4$ reduction case (Figure 1c). UV/Vis spectroscopy measurement of the toluene solution in a range of 350 nm to 650 nm showed a peak wavelength and absorbance (Abs) of 395 nm and 0.76, respectively, which would correspond with the generation of $BV^0$ molecules as in a previous report (Figure 2b).[21] Indium metal is critical for generating $BV^0$; a control experiment revealed that an inefficient and different reaction product was identified without indium metal (the temperature was the same, 60 °C) (Figures 2b and S1). In the case not using the indium fragment, the peak wavelength and Abs were ~429 nm and ~0.15, respectively. Temperature is also critical to obtaining the $BV^0$ molecules. As shown in Figures 2b and S1, the sample placed at room temperature for 24 hours after adding an indium fragment showed almost no color change, both in the bottom aqueous and top toluene layers, while a slight violet color was observed around the metal surface, indicating the inefficient generation of the monovalent form of benzyl viologen ($BV^+$). Accordingly, both incorporation of indium metal and heating would be critical to generating $BV^0$ molecules.

To further understand the reaction scheme, we examined the reaction system with other metals, such as manganese and aluminum (Figures 2c and 2d). The UV/Vis spectrum of the reacted solution with manganese showed a peak at 407 nm with an Abs of ~2.2; therefore, the $BV^0$ molecules would be generated using manganese as well (Figure 2c). To understand why the reaction proceeds in the indium and manganese cases, the standard reduction potential was considered. In the case of indium, $In_2O_3$/In, $In(OH)_4^-$/In, and $In(OH)_3$/In redox pairs showed the reduction potential about −1 V vs. standard hydrogen electrode (SHE),[25] which was more negative than $BV^{2+}/BV^+$ and $BV^+/BV^0$ redox pairs of −0.36 V and −0.58 V,[26] respectively, vs. SHE (Figure 2e). Indications of a continuous reaction were observed, indicating that the aqueous-soluble $In(OH)_4^-$ might have been generated. In the case of manganese, $Mn(OH)_2$/Mn and $Mn^{2+}$/Mn redox pairs have a high negative reduction potential, as −1.56 V and −1.19 V, respectively, vs.[25] SHE. From this perspective, aluminum, with a high reduction potential of less than −1.6 V vs. SHE,[25] would also be a good candidate for preparing $BV^0$. Contrary to the expectation, the reaction with aluminum generated pale yellow in toluene with a ~430 nm peak and a low Abs of ~0.18 on the UV/Vis spectrum (Figures 2d, S2, S3), which is similar to the reaction result without indium (Figures 2b and S1). The Al fragment showed an initial reaction forming $BV^+$ (violet stream); however, the reaction stopped after a while (Figure S2). This behavior would have been due to the passivation of the aluminum surface with aluminum oxide. In fact, the fresh surface of the Al shows the reactivity to form a $BV^+$ violet stream, and the larger the fresh surface area of the tiny Al fragments shows apparent reaction to form the $BV^+$ violet stream. On the other hand, the aged (as-obtained and non-treated) Al surface, which would be covered with oxide, shows no reactivity (Figure S2). According to the observations, the reduction potential of the metals would have been a key factor in generating the reduced form of BV isomers, and the metals of indium and manganese further progressed the reaction to form the two-electron reduced $BV^0$ molecules.

The extracted $BV^0$ molecules in the toluene solution (from indium-based synthesis) was treated for a bulk-$MoS_2$ MOSFETs (Figure 3a). The $MoS_2$ was mechanically exfoliated on a 260 nm thermally grown $SiO_2$ on $p^+$-Si wafer, and the device was fabricated with a standard lithographic technique. The original

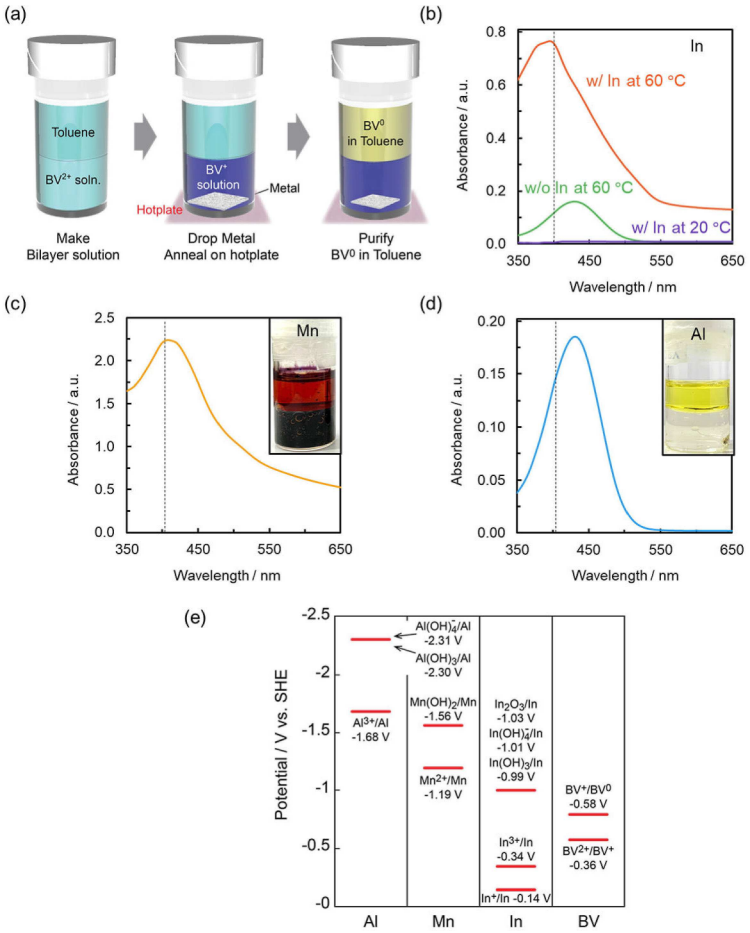


**Figure 2.** (a) Illustrative image of the experimental procedure on a hotplate. (b) UV/Vis spectra for the extracted toluene layer 24 h after the reaction. Each curve shows the synthesized solution with an indium plate at 60 °C, without an indium plate at 60 °C, and with an indium plate at 20 °C. (c, d) UV-Vis spectrum of the 24 h-reacted toluene solution. The reaction is processed with (c) manganese and (d) aluminum. The inset is the picture of the solution obtained after the 24 h reaction. The reaction solutions are bubbled with $N_2$ gas beforehand. (e) Reduction potentials of Al, Mn, In and BV molecules in respect to the standard hydrogen electrode (SHE).

device showed usual n-type behavior with an ON/OFF ratio in the drain current ($I_D$) of ~4 in a range of applying gate voltage ($V_G$) between −30 V and 30 V (Figure 3a). The output characteristic curves also show the gate dependency of the MOSFET (Figure S4). The treated MOSFET with the synthesized $BV^0$ (toluene solution from indium-based synthesis) showed completely different electrostatic behaviors; a higher drain current with a small gate dependency was observed, indicating that the synthesized molecules dope electrons strongly to the $MoS_2$ MOSFET which is close to a metallic state. To further confirm the electron transfer doping, a monolayer $MoS_2$ was treated with the synthesized molecules. With the treatment, the Raman signal of the A′ mode (out-of-plane vibration) shifted to a lower energy, while the Raman signal of the E′ mode (in-plane vibration) was maintained, which is consistent with previous reports of electron doping with $BV^0$ molecules synthesized using $NaBH_4$ (Figure 3b).[15] The photoluminescence (PL) spectrum after the treatment showed a red shift from the original (as-exfoliated monolayer $MoS_2$), indicating a larger contribution of a charged-exciton (trion) signal, around 1.84 eV, by increasing the carrier concentrations (Figure 3c).[14] The molecules generated with the manganese showed a behavior similar to that of the molecules generated in the indium case (Figure S4). According to the above results, the metal-based reduction systems effectively generated a strong electron dopant of the $BV^0$ molecule, which was confirmed by $MoS_2$ MOSFETs, and Raman and PL spectroscopy.

We found that $N_2$ bubbling applied to the solution prior to the reaction is important to effectively prepare the neutral $BV^0$ molecules. As shown in Figure 4a, the bottom aqueous solution was not filled with a violet color of $BV^+$ when the solution was not bubbled with $N_2$ gas in advance; rather, only a tiny stream of $BV^+$ was observed. In a previous study, monovalent radical viologen species reacted with oxygen to form several chemical species and generate a yellow-colored solution.[24] The yellow-colored solution of the upper toluene layer shows a signal around 420–430 nm that is red-shifted from the solution with $N_2$ bubbling (Figures 4b and S3). To identify whether it is a $BV^0$ molecule, the toluene solution in Figure 4a was applied to a $MoS_2$ MOSFET (Figure 4c). Even after the treatment process (immersion in the toluene solution) for 24 hours, the MOSFET showed an ON/OFF ratio of ~3; rather, the $I_D$ at $V_G = 30$ V

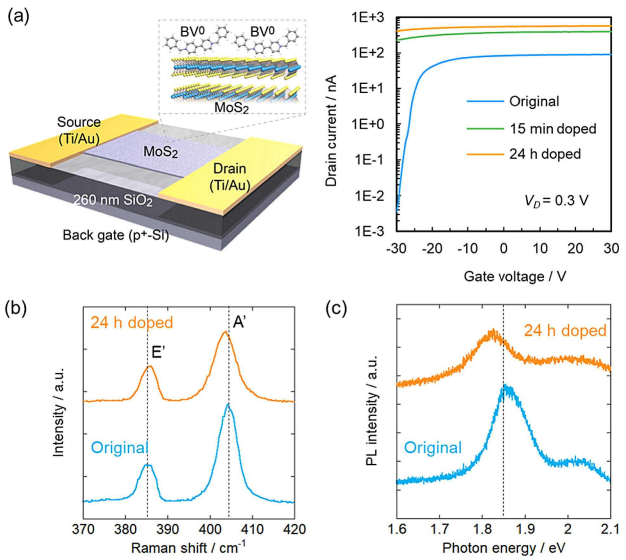


**Figure 3.** (a) Illustration of the MOSFET device with $MoS_2$ treated with $BV^0$ molecules on the surface and the transfer characteristic curves for the original (not $BV^0$ doped), 15 min doped, and 24 h doped. (b) Raman spectra for the original and 24 h doped of the monolayer $MoS_2$. (c) PL spectra for the original and 24 h doped of the monolayer $MoS_2$. All the dopants were prepared with indium on a hotplate at 60 °C. The solutions are bubbled with $N_2$ gas.

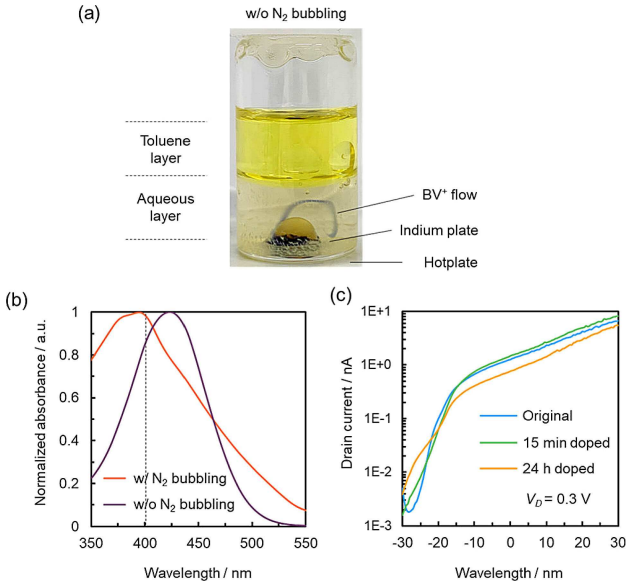


**Figure 4.** (a) The picture of the 24 h-reacted solution with an indium plate on a hotplate at 60 °C without $N_2$ bubbling beforehand. (b) Normalized UV-Vis spectra for the toluene solution of the 24 h reaction without $N_2$ bubbling. As a comparison, the solution with $N_2$ bubbled shown in Figure 2b is also plotted. (c) The transfer characteristic curves for the $MoS_2$ MOSFET by the treatment with the 24 h reacted toluene solution (without $N_2$ bubbling) on it. The curves are the original, and the 15 min doped and 24 h doped samples.

decreases slightly with increasing the treatment time. Therefore, the molecules generated *via* the process without $N_2$ bubbling were different from the electron dopant $BV^0$; most likely the product was an oxygen-reacted species.

The reaction system without $N_2$ bubbling is useful as a visualization model for the reaction, because the lifetime of the violet $BV^+$ generated from the metal surface in the aqueous solution is limited. Additionally, the solution is transparent; as such, the streamline in the vial can be visualized (as shown in Figures 1d and 4a). Furthermore, the generated neutral molecules (most likely oxygen-reacted species), which were extracted in the upper toluene layer (meaning they are hydrophobic neutral molecules), would be useful as a model for analyzing the generated hydrophobic $BV^0$ molecules in the aqueous solution.

Since the $BV^0$ is a neutral molecule, solvation in water is limited.[21] It requires a transportation mechanism of the generated $BV^0$ molecules from the metal surface at the bottom aqueous solution to the upper toluene layer. We considered the macroscopic behavior of the reaction solution by comparing two heating systems of 1) a hotplate that generated a large temperature gradient (Figure 5a) and 2) heating the reaction vial uniformly in an oven with a small temperature gradient (Figure 5b). The temperatures of the surface on the hotplate and in the oven were 60 °C. The heating on the hotplate showed a convection flow (Figure 1d) and generated $BV^0$ in the upper toluene layer (Figures 1c and 2b). On the other hand, heating the vial uniformly in an oven, a diffusion of $BV^+$ above the indium surface was observed (Figure 5c, and the illustrative image is Figure 5b). Twenty-four hours after the reaction, the bottom aqueous layer showed a dark purple solution, indicating a large amount of $BV^+$ generation similar to that of heating on a hotplate, while the upper toluene layer showed a pale-yellow solution (Figure 5d). Figure 5e showed a UV/Vis spectrum for the toluene layer generated by the uniform heating in the oven, and the Abs was just 0.04 at 399 nm. The spectrum in toluene layer of the synthesis in the oven showed $BV^0$ generation, but the Abs was 1/19 of the process on the hotplate. Since Abs is proportional to the concentration of the product, the generation rate of $BV^0$ was 1/19 *via* heating in the oven compared to heating on the hotplate.

The difference between the heating conditions was the temperature distribution at the bottom and top of the vial (Figure 5a and b). Convection flow (known as Rayleigh-Bénard convection) can be generated by a certain temperature difference ($\Delta T$) between the top and bottom of the vial, generating a denser liquid in the top that flows down to the bottom.[27–29] This phenomenon is evaluated with Rayleigh number (Ra)[27,29] as

$$\mathrm{Ra} = \frac{g\beta\Delta T L^3}{v\alpha} \quad (1)$$

where g, β, v, α, and $L$ are the acceleration of gravity, the thermal expansion coefficient, the kinematic viscosity, the thermal diffusivity, and the system length, respectively. The critical Ra is known to be 1,708;[29] above that point, the instability and the convection flow is generated. Figure S5 shows the estimated Ra vs. $\Delta T$ curve in water, and that the convection flow would be generated even with a small temperature distribution ($\Delta T$ over ~0.03 °C from equation (1)). All

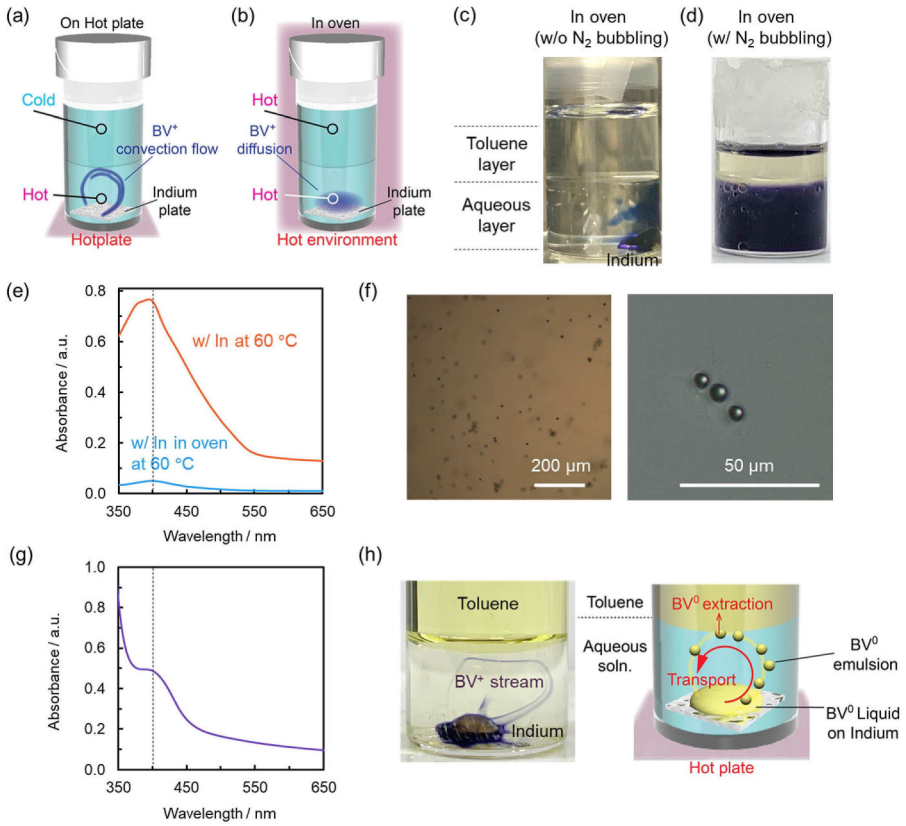


**Figure 5.** (a, b) Illustrations of the setups for the two heating scenarios in this work. (a) The heating on the hotplate for the processes in Figures 1 to 4. Temperature gradient is expected. (b) In-oven experiment shows a uniform heating of the vial. (c) The picture of the 1 h-reacted solution in the oven. The solution is not $N_2$ bubbled to visualize the dynamics of the solution. (d, e) The picture (d) and UV-Vis spectrum (e) of the 24 h-reacted solution in the oven. The solution is $N_2$ bubbled beforehand. As a comparison, the solution heated on the hotplate with $N_2$ bubbled (Figure 2b) is also plotted in (e). (f) Microscope images of the aqueous solution of the 24 h-reacted without $N_2$ bubbling to visualize. (g) The UV-Vis spectrum for the aqueous solution in Figure 5f. (h) The representative picture of the generated convection flow (the solution is not $N_2$ bubbled to visualize the dynamics, the picture is the 4 h-reacted solution) and the illustration of a plausible mechanism of the transportation of the $BV^0$ generated on the metal plate.

parameters except $\Delta T$ would have the same values in the two heating scenarios of the hotplate and the oven. In the hotplate scenario, the bottom temperature is higher than the top temperature, as illustrated in Figure 5a. Although the temperature distribution should be exhibited even in the heating in the oven, especially at the moment of placing the vial in the oven, the $\Delta T$ would be tiny after reaching a steady state, the convection flow would not be generated and the $BV^0$ molecules generated at the metal surface would have no way to transport to the upper toluene layer which was centimeter separated from the bottom. As a result, the system in the oven did not show an efficient generation of $BV^0$ dopant molecules.

To visualize the transportation on a microscopic scale, the aqueous solution on the hotplate was further analyzed. For this purpose, the analyzed sample used was the solution untreated by $N_2$ bubbling. Under a microscope, tiny droplets with a diameter of ~10 μm were observed, which was phase-separated from the aqueous solution (Figure 5f). The UV/Vis spectrum of the aqueous solution showed a signal around 400 nm, indicating that the generated droplet had been transported and produced the yellow toluene layer (Figures, 4a, b and 5 g). In the $N_2$ bubbling case, although it was difficult to visualize due to the dense $BV^+$ violet color (Figure 1c), the neutral $BV^0$ molecules would form a similar droplet by phase separation from water and be transported to the upper toluene layer by the convection flow. From the results above, the dopant molecule, $BV^0$, generated on the indium and manganese surfaces would be effectively transported by the non-equilibrium convection flow from the bottom solution to the upper hydrophobic toluene layer (Figure 5h); simultaneously in the transportation, the $BV^0$ molecules could be separated from $BV^{2+}$ and $BV^+$ isomers.

In summary, generation of the neutral $BV^0$ molecules with indium and manganese fragments as a metal-reduction system was demonstrated. The method was achieved by simply dropping the air-stable metal fragments into the vial. The generated $BV^0$ molecules effectively doped bulk $MoS_2$ MOSFETs and monolayer $MoS_2$, confirmed by MOSFET behavior, PL and Raman spectroscopy. In addition, the important finding is that the temperature gradient facilitates the transportation of the produced $BV^0$ molecules from the aqueous solution to the upper toluene layer by the generated convection flow, and simultaneous purification from the aqueous isomers of $BV^+$ and $BV^{2+}$ was incorporated. This synthetic method would be useful for the nanoelectronic fields of TMDCs, graphene and carbon nanotubes to achieve strong doping *via* the simple and easy

dopant-preparation system. Furthermore, the idea of using a double-layer with convection flow environment would be useful for isolating isomers of redox-active molecules such as viologen-based molecules or others to synthesize and purify simultaneously.

## Experimental Section

### Sample Preparation Process

Benzyl viologen dichloride ($BV^{2+}$ isomer, Sigma-Aldrich) was dissolved in Milli-Q water to prepare 7 mg/ml of solution. The toluene (Sigma-Aldrich) layer (2 ml) was placed on the $BV^{2+}$ aqueous solution of 2 ml and heated on a hotplate or in the oven. Both the toluene and the $BV^{2+}$ aqueous solutions were $N_2$ bubbled for 30 min each beforehand, and further bubbling was performed on the bilayer solution for 5 min. The heating was done under a dark condition. For heating in the oven, the vial was wrapped in aluminum foil. The surface temperature of the hotplate and the temperature in the oven were controlled and monitored in advance. Indium metal (Sigma-Aldrich) was pre-treated with 1% HCl and rinsed with Milli-Q water sufficiently before use. Manganese (The Nilaco Corporation) and Al (The Nilaco Corporation) were used as obtained. The metals were cut into pieces with a surface area of about 50 $mm^2$ for the indium and manganese, and 25–30 $mm^2$ for the aluminum. The indium and manganese were in platelet form, and the aluminum was in wired form. The metal plates were placed parallel to the ground at the bottom of the vial. All the reactions were done in a glass vial with an outer diameter of 18 mm. $MoS_2$ MOSFET was prepared by exfoliation of $MoS_2$ (SPI Supplies) on a $p^+$-Si wafer covered with a thermally grown 260 nm $SiO_2$ (Silicon Valley Microelectronics, Inc.). Source and drain contacts were constructed using Au/Ti (50 nm/3 nm), and fabricated using a standard lithography technique.

### Physical Measurements

Optical microscope observation was carried out with an Olympus BX51. UV/Vis spectra were obtained with a JASCO Co. V-650 spectrometer. The solutions were diluted with a neat solvent beforehand to be a quarter concentration of as prepared. Electrical characteristics were measured using a semiconductor parameter analyzer (Keysight, B1500a). Photoluminescence and Raman spectra were obtained using a LabRAM HR800 equipped with an EMCCD camera (HORIBA Scientific). The diameter of the incident beam was about 2 μm, and the laser power was ~27 $W\,cm^{-2}$ for Raman spectroscopy and 2.7 $W\,cm^{-2}$ for PL spectroscopy.

## Acknowledgements

*K. M. and A. F. are contributed equally to this work. This work was supported by JST PRESTO Grant No. JPMJPR1663 and Research Foundation for Opto-Science and Technology.*

## Conflict of Interest

The authors declare no conflict of interest.

**Keywords:** transition metal dichalcogenides · benzyl viologen · redox reactions · molecular doping · convection flow

[1] D. Jariwala, V. K. Sangwan, L. J. Lauhon, T. J. Marks, M. C. Hersam, *ACS Nano* **2014**, *8*, 1102.
[2] Q. H. Wang, K. Kalantar-Zadeh, A. Kis, J. N. Coleman, M. S. Strano, *Nat. Nanotechnol.* **2012**, *7*, 699.
[3] E. O. Marco Gobbi, Paolo Samorì, *Adv. Mater.* **2018**, 176103.
[4] M. Chhowalla, H. S. Shin, G. Eda, L. J. Li, K. P. Loh, H. Zhang, *Nat. Chem.* **2013**, *5*, 263.
[5] H. Schmidt, F. Giustiniano, G. Eda, *Chem. Soc. Rev.* **2015**, *44*, 7715.
[6] S. Bertolazzi, J. Brivio, A. Kis, *ACS Nano* **2011**, *5*, 9703.
[7] D. Lembke, A. Kis, *ACS Nano* **2012**, *6*, 10070.
[8] B. Radisavljevic, A. Radenovic, J. Brivio, V. Giacometti, A. Kis, *Nat. Nanotechnol.* **2011**, *6*, 147; *Nat. Mater.* **2013**, *12*, 815.
[9] T. Roy, M. Tosun, X. Cao, H. Fang, D.-H. Lien, P. Zhao, Y.-Z. Chen, Y.-L. Chueh, J. Guo, A. Javey, *ACS Nano* **2015**, *9*, 2071; D. Sarkar, X. Xie, W. Liu, W. Cao, J. Kang, Y. Gong, S. Kraemer, P. M. Ajayan, K. Banerjee, *Nature* **2015**, *526*, 91.
[10] W. Choi, M. Y. Cho, A. Konar, J. H. Lee, G.-B. Cha, S. C. Hong, S. Kim, J. Kim, D. Jena, J. Joo, S. Kim, *Adv. Mater.* **2012**, *24*, 5832; O. Lopez-Sanchez, D. Lembke, M. Kayci, A. Radenovic, A. Kis, *Nat. Nanotechnol.* **2013**, *8*, 497.
[11] A. Pospischil, M. M. Furchi, T. Mueller, *Nat. Nanotechnol.* **2014**, *9*, 257; D. Jariwala, A. R. Davoyan, J. Wong, H. A. Atwater, *ACS Photonics* **2017**, *4*, 2962; M. M. Furchi, A. Pospischil, F. Libisch, J. Burgdörfer, T. Mueller, *Nano Lett.* **2014**, *14*, 4785.
[12] B. W. H. Baugher, H. O. H. Churchill, Y. Yang, P. Jarillo-Herrero, *Nat. Nanotechnol.* **2014**, *9*, 262; J. S. Ross, P. Klement, A. M. Jones, N. J. Ghimire, J. Yan, D. G. Mandrus, T. Taniguchi, K. Watanabe, K. Kitamura, W. Yao, D. H. Cobden, X. Xu, *Nat. Nanotechnol.* **2014**, *9*, 268.
[13] B. Liu, L. Chen, G. Liu, A. N. Abbas, M. Fathi, C. Zhou, *ACS Nano* **2014**, *8*, 5304; L. Yang, K. Majumdar, H. Liu, Y. Du, H. Wu, M. Hatzistergos, P. Y. Hung, R. Tieckelmann, W. Tsai, C. Hobbs, P. D. Ye, *Nano Lett.* **2014**, *14*, 6275; H. Ichimiya, M. Takinoue, A. Fukui, K. Miura, T. Yoshimura, A. Ashida, N. Fujimura, D. Kiriya, *ACS Nano* **2018**, *12*, 10123; H. Fang, S. Chuang, T. C. Chang, K. Takei, T. Takahashi, A. Javey, *Nano Lett.* **2012**, *12*, 3788; S. Zhang, H. M. Hill, K. Moudgil, C. A. Richter, A. R. Hight Walker, S. Barlow, S. R. Marder, C. A. Hacker, S. J. Pookpanratana, *Adv. Mater.* **2018**, *30*, 1802991.
[14] S. Mouri, Y. Miyauchi, K. Matsuda, *Nano Lett.* **2013**, *13*, 5944.
[15] D. Kiriya, M. Tosun, P. Zhao, J. S. Kang, A. Javey, *J. Am. Chem. Soc.* **2014**, *136*, 7853.
[16] Y. Joo, M. Kim, C. Kanimozhi, P. Huang, B. M. Wong, S. S. Roy, M. S. Arnold, P. Gopalan, *J. Phys. Chem. C*, **2016**, *120*, 13815.
[17] C. Huang, M. Kim, B. M. Wong, N. S. Safron, M. S. Arnold, P. Gopalan, *J. Phys. Chem. C*, **2014**, *118*, 2077.
[18] H. L. Yuchen Du, Adam T. Neal, Mengwei Si, Peide D. Ye, *IEEE Electron Device Lett.* **2013**, *34*, 1328.
[19] J. D. Lin, C. Han, F. Wang, R. Wang, D. Xiang, S. Qin, X. A. Zhang, L. Wang, H. Zhang, A. T. Wee, W. Chen, *ACS Nano* **2014**, *8*, 5323; D. Kiriya, Y. Zhou, C. Nelson, M. Hettick, S. R. Madhvapathy, K. Chen, P. Zhao, M. Tosun, A. M. Minor, D. C. Chrzan, A. Javey, *Adv. Funct. Mater.* **2015**, *25*, 6257.
[20] H. Fang, M. Tosun, G. Seol, T. C. Chang, K. Takei, J. Guo, A. Javey, *Nano Lett.* **2013**, *13*, 1991.

[21] S. M. Kim, J. H. Jang, K. K. Kim, H. K. Park, J. J. Bae, W. J. Yu, I. H. Lee, G. Kim, D. D. Loc, U. J. Kim, E.-H. Lee, H.-J. Shin, J.-Y. Choi, Y. H. Lee, *J. Am. Chem. Soc.* **2009**, *131*, 327.
[22] H.-M. Li, D. Lee, D. Qu, X. Liu, J. Ryu, A. Seabaugh, W. J. Yoo, *Nat. Commun.* **2015**, *6*, 6564.
[23] W. J. Yu, L. Liao, S. H. Chae, Y. H. Lee, X. F. Duan, *Nano Lett.* **2011**, *11*, 4759.
[24] C. D. Clark, J. D. Debad, E. H. Yonemoto, T. E. Mallouk, A. J. Bard, *J. Am. Chem. Soc.* **1997**, *119*, 10525.
[25] *CRC Handbook of Chemistry and Physics, 94th ed.*, CRC Press, Boca Raton, FL 2013–2014.
[26] T. Kawata, M. Yamamoto, M. Yamana, M. Tajima, T. Nakano, *J. J. Appl. Phys.* **1975**, *14*, 725.
[27] M. Krishnan, V. M. Ugaz, M. A. Burns, *Science* **2002**, *298*, 793.
[28] T. H. Solomon, J. P. Gollub, *Phys. Rev. A* **1988**, *38*, 6280.
[29] A. Pandey, J. D. Scheel, J. Schumacher, *Nat. Commun.* **2018**, *9*, 2118.

Manuscript received: May 11, 2019
Revised manuscript received: June 12, 2019